Constant Modulus Waveform Design for MIMO Radar Transmit Beampattern

Ziyang Cheng, Zishu He, *Member, IEEE*, Shengmiao Zhang, and Jian Li, *Fellow, IEEE*

***Abstract*—A multiple-input multiple-output radar has great flexibility to design the transmit beampattern via selecting the probing waveform. The idea of current transmit beampattern design is to approximate the disired transimit beampattern and minimize the cross-correlation sidelobes. In this paper, under the constant modulus constraint, two algorithms are proposed to design the probing waveform directly. In the first algorithm, the optimization criterion is minimizing the squared-error between the designed beampattern and the given beampattern. Since the objective function is a nonconvex fourth-order polynomial and the constant modulus constraint can be regarded as many nonconvex quadratic equality constraints, an efficient alternating direction method of multipliers (ADMM) algorithm, whose convergence speed is very fast, is proposed to solve it. In the second algorithm, the criterion is minimizing the absolute-error between the designed beampattern and the given beampattern. This nonconvex problem can be formulated as l_1-norm problem, which can be solved through a double-ADMM algorithm. Finally, we assess the performance of the two proposed algorithms via numerical results.**

***Index Terms*—Constant modulus waveform, transmit beampattern design, MIMO radar, ADMM, DADMM.**

I. Introduction

IT IS well known that multiple-input multiple-output (MIMO) radar systems have the capability to transmit independent waveforms out of each transmit antenna. Taking advantage of this waveform diversity, MIMO radars can obtain a higher spatial resolution and a better detection performance compared with a strandard phased-array radar [1]–[5]. Generally, a MIMO radar system can be classified into two categories depending on the distribution position of the antennas: distributed MIMO radars [6]–[8] and colocated MIMO radars [9], [10]

Recently, the waveform design for MIMO radar has been widely studied. The main approaches can be generally classified into the following categories. The first category is developed to devise the waveform for distributed MIMO radar by maximizing the mutual information (MI) between the received echoes and the target response [11], [12]. The second category addresses the problem of waveform design in the presence of signal dependence clutter. In these works, an iterative approach is presented to jointly optimize the transmit waveform and receive filter to maximize the output signal-to-interference-plus-noise ratio (SINR) [13]–[18]. The third category solves the MIMO radar beampattern synthesis problem. The core issue of this problem is to control the spatial distribution of the transmit power. For example, in [19], the authors devise the waveform covariance matrix $\mathbf{R}$ to match the desired pattern through semidefinite quadratic programming (SQP) technique, and then a cyclic algorithm (CA) is proposed in [20] to synthesis the constant modulus waveform matrix $\mathbf{X}$ to approximate the covariance matrix $\mathbf{R}$. The CA approach is also applied to the synthesis of constant-modulus transmit signals with good auto- and cross-correlation properties [21]. In [22], the authors have proposed a closed-form covariance matrix design method to achieve the desired beampattern based on discrete-Fourier-transform (DFT) coefficients and Toeplitz matrices. [23] and [24] have extended the DFT-based technique to a planar-antenna-array, and also presented a direct constant-envelope waveforms design algorithm for the desired beampattern. The DFT-based technique achieves transmit beampattern match at low complexity. However, the drawback of the DFT-based method is that, for small number of antennas, the performance of the DFT-based method is slightly poorer. In addition, comparing to the squared-error criterion, [25] has developed the better beampattern design method using the absolute-error criterion. However, it can not realize the direct waveform matrix $\mathbf{X}$ design. Other literatures on transmit beampattern synthesis, readers can refer to [26]–[29].

Unlike the existing two-step method (first optimize the waveform correlation matrix $\mathbf{R}$ and then design the transmit waveform matrix $\mathbf{X}$ using $\mathbf{R}$), in this paper, by considering the constant modulus constraint, we present two novel approaches to design the transmit waveform vector $\mathbf{s}$ directly. In the first proposed approach, the cost-function is the squared-error between the designed beampattern and the desired beampattern. We formulate the problem as a minimization of a fourth-order polynomial subject to nonconvex constant mudulus constraint [30]. Whereas the efficient direct solution to this kind of problem is rarely discussed in previous literatures. In this work, we first convert the problem to the bi-convex problem, and then solve it based on a effective technique known as the alternating

Manuscript received January 26, 2017; revised May 1, 2017 and June 3, 2017; accepted June 13, 2017. Date of publication June 22, 2017; date of current version July 17, 2017. The associate editor coordinating the review of this manuscript and approving it for publication was Prof. Hongbin Li. *(Corresponding author: Ziyang Cheng.)*

Z. Cheng and Z. He are with the School of Electronic Engineering, University of Electronic Science and Technology of China, Chengdu 611731, China (e-mail: zeeyoungcheng@163.com; zshe@uestc.edu.cn).

S. Zhang is with the Science and Technology on Electronic Information Control Laboratory, Chengdu 610036, China (e-mail: miaomiao871@sina.com).

J. Li is with the Department of Electrical and Computer Engineering, University of Florida, Gainesvile, FL 32611-6130 USA (e-mail: li@dsp.ufl.edu).

Color versions of one or more of the figures in this paper are available online at http://ieeexplore.ieee.org.

Digital Object Identifier 10.1109/TSP.2017.2718976

1053-587X © 2017 IEEE. Personal use is permitted, but republication/redistribution requires IEEE permission.
See http://www.ieee.org/publications_standards/publications/rights/index.html for more information.

Authorized licensed use limited to: UNIVERSITA MODENA. Downloaded on May 18,2024 at 12:47:07 UTC from IEEE Xplore. Restrictions apply.

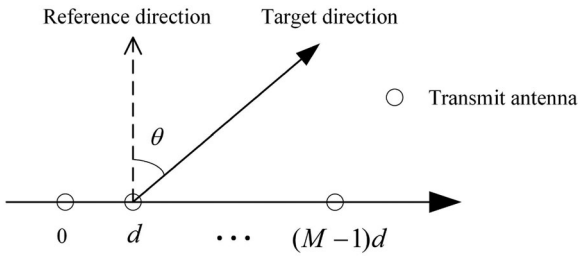

Fig. 1. Colocated MIMO radar with M antennas (ULA). θ is the direction of interest.

direction method of multipliers (ADMM) algorithm [31]–[34], and a close-form solution to each iteration of the ADMM can be easily obtained. The cost-function of the second approach is the absolute-error between the designed beampattern and the given beampattern. Since the formulated problem is also an intractable nonconvex problem, we first formulate the problem as a l_1-norm problem by introducing an auxiliary variable, then a double-ADMM (DADMM) algorithm is presented to solve it. The proposed ADMM algorithms are different from the typical ADMM algorithm since the constraints in the considered models are non-linear. More importantly, the two proposed algorithms can be efficiently solved without the CVX toolbox [36]. Finally, the two proposed algorithms are compared with the existing approaches in terms of the beampattern performance via numerical results.

The organization of this paper is as follows. The system model for colocated MIMO radars and the problem formulations are presented in Section II. The first algorithm is introduced in Section III and the second algorithm is introduced in Section IV. Section V presents our numerical results. Finally, our conclusions are drew in Section VI.

Notation: Lower case letters $\mathbf{a}$ and upper case letters $\mathbf{A}$ denote vectors and matrices, respectively. The symbols $(\cdot)^T$, $(\cdot)^\dagger$ and $(\cdot)^*$, respectively, stand for the transpose, the conjugate transpose and the conjugate operators. The n-th element of a vector $\mathbf{a}$ is written as $a(n)$. $\mathrm{vec}(\mathbf{A})$ denotes the column vector of matrix $\mathbf{A}$. The sets of $N \times N$ complex matrices and the sets of n-dimensional complex numbers vectors are denoted by $\mathbb{C}^{N\times N}$ and $\mathbb{C}^n$, respectively. The l_2 norm and the l_1 norm are always, respectively, denoted by the symbols $\|\cdot\|_2$ and $\|\cdot\|_1$. We let $\mathbf{I}_N$ stand for the identity matrix of size $N \times N$. Finally, we use $\mathrm{Re}\{x\}$ and $\mathrm{Im}\{x\}$ for the real part and the imaginary part of x, respectively, and the symbol $\otimes$ for Kronecker product.

II. System Model and Problem Formulation

A. System Model

A colocated MIMO radar with M transmit antennas in a uniform linear array (ULA) is considered, as shown in Fig. 1. We let $s_i(l), i = 1, 2, \cdots, M; l = 1, 2, \cdots, L$ denote the discrete time waveform emited by the i-th transmit antenna, where L is the number of samples of each transmit pulse. Let $\mathbf{s}_l = [s_1(l), s_2(l), \ldots, s_M(l)]^T$ be a M-dimensional vector which collects M transmit waveforms of the l-th sample, and $\mathbf{S} = [\mathbf{s}_1, \mathbf{s}_2, \ldots, \mathbf{s}_L] \in \mathbb{C}^{M\times L}$ is the space-time transmit waveform matrix.

The synthesis signal seen at the direction θ is given by

$$x(l) = \mathbf{a}_T^T(\theta)\mathbf{s}_l, l = 1, 2, \ldots, L, \tag{1}$$

where

$$\mathbf{a}_T(\theta) = [1, e^{-j2\pi d\mathrm{u}/\lambda}, \ldots, e^{-j2\pi(M-1)d\mathrm{u}/\lambda}]^T \tag{2}$$

denotes the M-dimensional transmit steering vector. d is the inter-element spacing, λ is the signal wavelength, and $\mathrm{u} = \sin\theta$ is the direction cosines.

Concatenating L samples synthesis signals in a vector $\mathbf{x}$, defined as

$$\begin{aligned}\mathbf{x} &= [x(1), x(2), \ldots, x(L)]^T \\ &= \left(\mathbf{I}_L \otimes \mathbf{a}_T^T(\theta)\right)\mathbf{s},\end{aligned} \tag{3}$$

where $\mathbf{s} = \mathrm{vec}(\mathbf{S})$. So, the power received at direction θ can be written as

$$\begin{aligned}P(\theta) &= \mathbf{x}^\dagger\mathbf{x} \\ &= \mathbf{s}^\dagger\left(\mathbf{I}_L \otimes \mathbf{a}_T^T(\theta)\right)^\dagger\left(\mathbf{I}_L \otimes \mathbf{a}_T^T(\theta)\right)\mathbf{s} \\ &= \mathbf{s}^\dagger\mathbf{R}(\theta)\mathbf{s},\end{aligned} \tag{4}$$

where

$$\mathbf{R}(\theta) = \left(\mathbf{I}_L \otimes \mathbf{a}_T^T(\theta)\right)^\dagger\left(\mathbf{I}_L \otimes \mathbf{a}_T^T(\theta)\right). \tag{5}$$

and the cross-correlation sidelobes is defined by

$$\begin{aligned}P_{cc}(\theta, \bar{\theta}) &= \mathbf{s}^\dagger\left(\mathbf{I}_L \otimes \mathbf{a}_T^T(\theta)\right)^\dagger\left(\mathbf{I}_L \otimes \mathbf{a}_T^T(\bar{\theta})\right)\mathbf{s} \\ &= \mathbf{s}^\dagger\bar{\mathbf{R}}(\theta, \bar{\theta})\mathbf{s},\end{aligned} \tag{6}$$

(for $\theta \neq \bar{\theta}$), where

$$\bar{\mathbf{R}}(\theta, \bar{\theta}) = \left(\mathbf{I}_L \otimes \mathbf{a}_T^T(\theta)\right)^\dagger\left(\mathbf{I}_L \otimes \mathbf{a}_T^T(\bar{\theta})\right). \tag{7}$$

B. Problem Formulation

In order to approximate the desired transmit beampattern and minimize the cross-correlation sidelobes, two cost functions are given in this subsection. The squared-error between the designed beampattern and the given beampattern is selected as the cost function in the previous works [19], which involves a beampattern matching term and a cross-correlation term. Therefore, the first cost function in this paper can be formulated as follow:

$$\begin{aligned}J_1(\alpha, \mathbf{s}) = &\frac{1}{K}\sum_{k=1}^{K}\omega_k\left|\alpha^2 d(\theta_k) - \mathbf{s}^\dagger\mathbf{R}(\theta_k)\mathbf{s}\right|^2 \\ &+ \frac{\omega_c}{\bar{K}^2 - \bar{K}}\sum_{p=1}^{\bar{K}-1}\sum_{q=p+1}^{\bar{K}}\left|\mathbf{s}^\dagger\bar{\mathbf{R}}(\theta_p, \theta_q)\mathbf{s}\right|^2,\end{aligned} \tag{8}$$

where $\omega_k \geq 0, k = 1, 2, \ldots, K$ is the weighted coefficient of the k-th point. α^2 is a scaling parameter to be optimized, and ω_c defines the weight for cross-correlation sidelobes. $d(\theta)$ represents the desired beampattern.

Authorized licensed use limited to: UNIVERSITA MODENA. Downloaded on May 18,2024 at 12:47:07 UTC from IEEE Xplore. Restrictions apply.

To simplify notations, equation (8) can be expressed as the following more compact form

$$J_1(\mathbf{r}) = \frac{1}{K}\sum_{k=1}^{K}\omega_k\left|\mathbf{r}^\dagger\mathbf{A}(\theta_k)\mathbf{r}\right|^2 + \frac{\omega_c}{\bar{K}^2-\bar{K}}\sum_{p=1}^{\bar{K}-1}\sum_{q=p+1}^{\bar{K}}\left|\mathbf{r}^\dagger\bar{\mathbf{A}}(\theta_p,\theta_q)\mathbf{r}\right|^2, \quad (9)$$

where

$$\mathbf{r} \triangleq \begin{pmatrix}\alpha\\ \mathbf{s}\end{pmatrix} \quad (10)$$

$$\mathbf{A}(\theta_k) \triangleq \begin{pmatrix} d(\theta_k) & \mathbf{0}^T\\ \mathbf{0} & -\mathbf{R}(\theta_k)\end{pmatrix} \quad (11)$$

and

$$\bar{\mathbf{A}}(\theta_p,\theta_q) \triangleq \begin{pmatrix} 0 & \mathbf{0}^T\\ \mathbf{0} & \bar{\mathbf{R}}(\theta_p,\theta_q)\end{pmatrix} \quad (12)$$

It is obvious that equation (9) is a nonconvex fourth-order polynomial depending on $\mathbf{r}$, which is a difficult NP-hard problem [29].

Meanwhile, the absolute-error cost functions provide a more robust fitting than the squared-error cost functions when the samples contain large outliers [30]. We also consider the cross-correlation term just as [25]. Hence, we provide the second cost function as follows:

$$J_2(\alpha,\mathbf{s}) = \frac{1}{K}\sum_{k=1}^{K}\omega_k\left|\alpha^2 d(\theta_k) - \mathbf{s}^\dagger\mathbf{R}(\theta_k)\mathbf{s}\right| + \frac{\omega_c}{\bar{K}^2-\bar{K}}\sum_{p=1}^{\bar{K}-1}\sum_{q=p+1}^{\bar{K}}\left|\mathbf{s}^\dagger\bar{\mathbf{R}}(\theta_p,\theta_q)\mathbf{s}\right|^2. \quad (13)$$

Similarly, equation (13) can be simplified as,

$$J_2(\mathbf{r}) = \frac{1}{K}\sum_{k=1}^{K}\omega_k\left|\mathbf{r}^\dagger\mathbf{A}(\theta_k)\mathbf{r}\right| + \frac{\omega_c}{\bar{K}^2-\bar{K}}\sum_{p=1}^{\bar{K}-1}\sum_{q=p+1}^{\bar{K}}\left|\mathbf{r}^\dagger\bar{\mathbf{A}}(\theta_p,\theta_q)\mathbf{r}\right|^2. \quad (14)$$

Constant modulus constraint prevents the non-linearity distortion of the power amplifier to maximize the efficiency of the transmitter. Specifically, considering the normalized envelope of the waveform vector $\mathbf{s}$, *i.e.*,

$$|s(i)| = 1,\ i = 1,\ 2,\ \ldots,\ ML. \quad (15)$$

It is straightforward to prove that equation (15) is equivalent to

$$\mathbf{r}^\dagger\mathbf{E}_{i+1}\mathbf{r} = 1,\ i = 1,\ 2,\ \ldots,\ ML, \quad (16)$$

where $\mathbf{E}_i$ is a square matrix with the size of $(ML+1)\times(ML+1)$, and all elements are 0 except the (i,i)-th element equal to 1.

Based on the aforementioned analysis, two optimization problems can be formulated in this paper,

$$\min_{\mathbf{r}}\ \frac{1}{K}\sum_{k=1}^{K}\omega_k\left|\mathbf{r}^\dagger\mathbf{A}(\theta_k)\mathbf{r}\right|^2 + \frac{\omega_c}{\bar{K}^2-\bar{K}}\sum_{p=1}^{\bar{K}-1}\sum_{q=p+1}^{\bar{K}}\left|\mathbf{r}^\dagger\bar{\mathbf{A}}(\theta_p,\theta_q)\mathbf{r}\right|^2 \quad s.t.\ \ \mathbf{r}^\dagger\mathbf{E}_{i+1}\mathbf{r} = 1, i = 1,2,\ldots,ML, \quad (17)$$

and

$$\min_{\mathbf{r}}\ \frac{1}{K}\sum_{k=1}^{K}\omega_k\left|\mathbf{r}^\dagger\mathbf{A}(\theta_k)\mathbf{r}\right| + \frac{\omega_c}{\bar{K}^2-\bar{K}}\sum_{p=1}^{\bar{K}-1}\sum_{q=p+1}^{\bar{K}}\left|\mathbf{r}^\dagger\bar{\mathbf{A}}(\theta_p,\theta_q)\mathbf{r}\right|^2 \quad s.t.\ \ \mathbf{r}^\dagger\mathbf{E}_{i+1}\mathbf{r} = 1, i = 1,2,\ldots,ML. \quad (18)$$

Since these two optimization models (17) and (18) both involve minimizing a nonconvex objective function and a nonconvex constant modulus equality constraint. They are NP-hard problems, and there has no effective method to solve these problems. Notice that the existing approaches to deal with the constant modulus constraint mainly include:

1) [19] first devises the waveform covariance matrix $\mathbf{R}$ subject to the diagonal elements of $\mathbf{R}$ equal to a constant, and then the constant modulus waveform $\mathbf{s}$ whose covariance matrix approximate $\mathbf{R}$ is obtained by using the cyclic algorithm (CA) [20];

2) The second approach to design the constant modulus waveform $\mathbf{s}$ consists of solving semidefinite programming (SDP) relaxation followed by a randomization technique. Readers interested in this aspect can refer to [13], [37], [38].

The above two methods are indirect methods and exist approximation error. In the following, two novel direct algorithms are proposed to solve the problem (17) and (18), respectively.

III. The First Algorithm

In this section, the algorithm to solve the problem (17) is presented. Here, we find a solution to (17) using a distributed optimization approach named alternation direction method of multipliers (ADMM) algorithm.

The ADMM algorithm blends the decomposability of dual ascent with the numerical robustness of the augmented Lagrangian method [31]. Based on the ADMM framework, we solve the nonconvex fourth-order polynomial function and nonconvex constant modulus constranit together.

A. Applying ADMM to (17)

We can decouple the fourth-order polynomial by introducing an auxiliary primal variable $\mathbf{h} \in \mathbb{C}^{ML+1}$, then, problem (17) is

Authorized licensed use limited to: UNIVERSITA MODENA. Downloaded on May 18,2024 at 12:47:07 UTC from IEEE Xplore. Restrictions apply.

equivalent to the following problem,

$$\min_{\mathbf{r},\mathbf{h}} \ \frac{1}{K}\sum_{k=1}^{K}\omega_k\left|\mathbf{h}^{\dagger}\mathbf{A}(\theta_k)\mathbf{r}\right|^2 + \frac{\omega_c}{\bar{K}^2-\bar{K}}\sum_{p=1}^{\bar{K}-1}\sum_{q=p+1}^{\bar{K}}\left|\mathbf{h}^{\dagger}\bar{\mathbf{A}}(\theta_p,\theta_q)\mathbf{r}\right|^2$$

$$s.t. \quad \mathbf{h}-\mathbf{r}=\mathbf{0}$$

$$\mathbf{h}^{\dagger}\mathbf{E}_{i+1}\mathbf{r}=1, i=1,2,\ldots,ML \tag{19}$$

The last ML equality constraints in problem (19) can be expressed in a unified compact form

$$\mathbf{G}(\mathbf{h},\mathbf{r})=\mathbf{0}, \tag{20}$$

where the vector $\mathbf{G}(\mathbf{h},\mathbf{r})\in\mathbb{C}^{ML}$ is given by

$$\begin{aligned}\mathbf{G}(\mathbf{h},\mathbf{r}) &= \mathbf{T}(\mathbf{h})\mathbf{r}-\mathbf{1}\\ &= \mathbf{T}'(\mathbf{r})\mathbf{h}-\mathbf{1},\end{aligned} \tag{21}$$

where

$$\mathbf{T}(\mathbf{h})=\left[\mathbf{h}^{\dagger}\mathbf{E}_2;\cdots;\mathbf{h}^{\dagger}\mathbf{E}_{ML+1}\right]\in\mathbb{C}^{ML\times ML+1}$$

and

$$\mathbf{T}'(\mathbf{r})=[\mathbf{E}_2\mathbf{r},\ldots,\mathbf{E}_{ML+1}\mathbf{r}]^{\dagger}\in\mathbb{C}^{ML\times ML+1}.$$

Notice that the objective function of problem (19) is bi-convex function, *i.e.*, it is convex in $\mathbf{h}$ for each $\mathbf{r}$ and convex in $\mathbf{r}$ for each $\mathbf{h}$. The equality constraint (20) is jointly affine in $\mathbf{h}$ and $\mathbf{r}$. Hence, the ADMM algorithm is very fit to be used in finding the solution to problem (19).

To simplify notations, we define,

$$F(\mathbf{h},\mathbf{r})=\frac{1}{K}\sum_{k=1}^{K}\omega_k\left|\mathbf{h}^{\dagger}\mathbf{A}(\theta_k)\mathbf{r}\right|^2 + \frac{\omega_c}{\bar{K}^2-\bar{K}}\sum_{p=1}^{\bar{K}-1}\sum_{q=p+1}^{\bar{K}}\left|\mathbf{h}^{\dagger}\bar{\mathbf{A}}(\theta_p,\theta_q)\mathbf{r}\right|^2 \tag{22}$$

To solve (19), we introduce two dual variables $\mathbf{y}\in\mathbb{C}^{ML+1}$ and $\mathbf{z}\in\mathbb{C}^{ML}$, the augmented Lagrangian of (19) is formed as

$$\mathcal{L}(\mathbf{h},\mathbf{r},\mathbf{y},\mathbf{z})=F(\mathbf{h},\mathbf{r})+\mathrm{Re}\{\mathbf{y}^{\dagger}(\mathbf{h}-\mathbf{r})\}+\frac{\rho_1}{2}\|\mathbf{h}-\mathbf{r}\|_2^2 + \mathrm{Re}\{\mathbf{z}^{\dagger}\mathbf{G}(\mathbf{h},\mathbf{r})\}+\frac{\rho_2}{2}\|\mathbf{G}(\mathbf{h},\mathbf{r})\|_2^2 \tag{23}$$

where $\rho_1,\rho_2>0$ are penalty parameters, which can be adjusted according to the design requirements.

At the $(m+1)$th iteration, the ADMM algorithm consists of the iterations,

$$\mathbf{h}^{m+1}:=\arg\min_{\mathbf{h}}\mathcal{L}(\mathbf{h},\mathbf{r}^m,\mathbf{y}^m,\mathbf{z}^m), \tag{24a}$$

$$\mathbf{r}^{m+1}:=\arg\min_{\mathbf{r}}\mathcal{L}(\mathbf{h}^{m+1},\mathbf{r},\mathbf{y}^m,\mathbf{z}^m), \tag{24b}$$

$$\mathbf{y}^{m+1}:=\mathbf{y}^m+\rho_1(\mathbf{h}^{m+1}-\mathbf{r}^{m+1}), \tag{24c}$$

$$\mathbf{z}^{m+1}:=\mathbf{z}^m+\rho_2\mathbf{G}(\mathbf{h}^{m+1},\mathbf{r}^{m+1}), \tag{24d}$$

Similar with the dual ascent approach, the ADMM algorithm also invovles the primal update and dual update. However, there are important differences between them. First of all, in the ADMM algorithm, the primal minimization steps use the augmented Lagrangian rather than the general Lagrangian, which ensure a faster convergence speed of the ADMM algorithm. Secondly, in the ADMM algorithm, the updates of (24a)–(24d) are executed in each iteration, instead of multiple updates until the convergence of inner loops in the dual ascent approach.

To solve (24a), it follows from (23),

$$\mathcal{L}(\mathbf{h},\mathbf{r}^m,\mathbf{y}^m,\mathbf{z}^m)=F(\mathbf{h},\mathbf{r}^m)+\frac{\rho_1}{2}\|\mathbf{h}-\mathbf{r}^m+\frac{1}{\rho_1}\mathbf{y}^m\|_2^2 + \frac{\rho_2}{2}\|\mathbf{G}(\mathbf{h},\mathbf{r}^m)+\frac{1}{\rho_2}\mathbf{z}^m\|_2^2+C \tag{25}$$

where C is a constant independent of $\mathbf{h}$. We denote $\mathbf{u}^m=\frac{1}{\rho_1}\mathbf{y}^m$ and $\mathbf{v}^m=\frac{1}{\rho_2}\mathbf{z}^m$ are the scaled dual variables, and inserting (21) into (24a) yields the following form,

$$\mathbf{h}^{m+1}:=\arg\min_{\mathbf{h}}\left\{\begin{array}{l}F(\mathbf{h},\mathbf{r}^m)+\frac{\rho_1}{2}\|\mathbf{h}-\mathbf{r}^m+\mathbf{u}^m\|_2^2\\ +\frac{\rho_2}{2}\|\mathbf{T}'(\mathbf{r}^m)\mathbf{h}-\mathbf{1}+\mathbf{v}^m\|_2^2\end{array}\right\} \tag{26}$$

Similarly, (24b)–(24d) can be writtern in a covenient form,

$$\mathbf{r}^{m+1}:=\arg\min_{\mathbf{r}}\left\{\begin{array}{l}F(\mathbf{h}^{m+1},\mathbf{r})+\frac{\rho_1}{2}\|\mathbf{h}^{m+1}-\mathbf{r}+\mathbf{u}^m\|_2^2\\ +\frac{\rho_2}{2}\|\mathbf{T}(\mathbf{h}^{m+1})\mathbf{r}-\mathbf{1}+\mathbf{v}^m\|_2^2\end{array}\right\} \tag{27}$$

$$\mathbf{u}^{m+1}:=\mathbf{u}^m+\mathbf{h}^{m+1}-\mathbf{r}^{m+1} \tag{28}$$

$$\mathbf{v}^{m+1}:=\mathbf{v}^m+\mathbf{T}'(\mathbf{r}^{m+1})\mathbf{h}^{m+1}-\mathbf{1} \tag{29}$$

Lemma 1: There are closed-form solutions in each iteration of $\mathbf{h}$ and $\mathbf{r}$. The $\mathbf{h}$-update is

$$\mathbf{h}^{m+1}=\mathbf{\Xi}^{-1}\boldsymbol{\gamma}, \tag{30}$$

where

$$\mathbf{\Xi}=\frac{1}{K}\sum_{k=1}^{K}\omega_k\mathbf{A}(\theta_k)\mathbf{r}^m\mathbf{r}^{m\,\dagger}\mathbf{A}^{\dagger}(\theta_k) + \frac{\omega_c}{\bar{K}^2-\bar{K}}\sum_{p=1}^{\bar{K}-1}\sum_{q=p+1}^{\bar{K}}\bar{\mathbf{A}}(\theta_p,\theta_q)\mathbf{r}^m\mathbf{r}^{m\,\dagger}\bar{\mathbf{A}}^{\dagger}(\theta_p,\theta_q) + \frac{\rho_1}{2}\mathbf{I}+\frac{\rho_2}{2}\mathbf{T}'^{\dagger}(\mathbf{r}^m)\mathbf{T}'(\mathbf{r}^m) \tag{31}$$

and

$$\boldsymbol{\gamma}=\frac{\rho_1}{2}(\mathbf{r}^m-\mathbf{u}^m)+\frac{\rho_2}{2}\mathbf{T}'^{\dagger}(\mathbf{r}^m)(\mathbf{1}-\mathbf{v}^m). \tag{32}$$

The $\mathbf{r}$-update is

$$\mathbf{r}^{m+1}=\mathbf{\Omega}^{-1}\boldsymbol{\zeta}, \tag{33}$$

Authorized licensed use limited to: UNIVERSITA MODENA. Downloaded on May 18,2024 at 12:47:07 UTC from IEEE Xplore. Restrictions apply.

where

$$\mathbf{\Omega} = \frac{1}{K}\sum_{k=1}^{K}\omega_k \mathbf{A}^{\dagger}(\theta_k)\mathbf{h}^{m+1}\mathbf{h}^{m+1\dagger}\mathbf{A}(\theta_k) + \frac{\omega_c}{\bar{K}^2-\bar{K}}\sum_{p=1}^{\bar{K}-1}\sum_{q=p+1}^{\bar{K}}\bar{\mathbf{A}}^{\dagger}(\theta_p,\theta_q)\mathbf{h}^{m+1}\mathbf{h}^{m+1\dagger}\bar{\mathbf{A}}(\theta_p,\theta_q) + \frac{\rho_1}{2}\mathbf{I} + \frac{\rho_2}{2}\mathbf{T}^{\dagger}(\mathbf{h}^{m+1})\mathbf{T}(\mathbf{h}^{m+1}) \quad (34)$$

and

$$\boldsymbol{\zeta} = \frac{\rho_1}{2}\left(\mathbf{h}^{m+1}-\mathbf{u}^m\right) + \frac{\rho_2}{2}\mathbf{T}^{\dagger}(\mathbf{h}^{m+1})(\mathbf{1}-\mathbf{v}^m). \quad (35)$$

Proof: The proof is provide in Appendix A. ■

B. Termination Criterions of the First Algorithm

We define

$$d_{r1}^{m+1} = \mathbf{h}^{m+1}-\mathbf{r}^{m+1},$$
$$d_{r2}^{m+1} = \mathbf{T}'(\mathbf{r}^{m+1})\mathbf{h}^{m+1}-\mathbf{1} \quad (36)$$

as the primal residuals at $m+1$ iteration and

$$d_s^{m+1} = \rho_1(\mathbf{r}^{m+1}-\mathbf{r}^m) \quad (37)$$

as dual residual at $m+1$ iteration, respectively. [30] suggests that a group of reasonable termination criterions are

$$\|d_{r1}^m\|_2^2 \le \epsilon_1^{pri}, \|d_{r2}^m\|_2^2 \le \epsilon_2^{pri} \quad \text{and} \quad \|d_s^m\|_2^2 \le \epsilon^{dual} \quad (38)$$

The tolerances for primal residuals ϵ_1^{pri}, ϵ_2^{pri} and dual residual ϵ^{dual} are defined in [30], such as,

$$\epsilon_1^{pri} = \sqrt{ML+1}\epsilon^{abs} + \epsilon^{rel}\max\{\|\mathbf{h}^m\|_2, \|-\mathbf{r}^m\|_2\}$$
$$\epsilon_2^{pri} = \sqrt{ML}\epsilon^{abs} + \epsilon^{rel}\max\{\|\mathbf{T}(\mathbf{h}^m)\mathbf{r}^m\|_2, \|-\mathbf{1}\|_2\}$$
$$\epsilon^{dual} = \sqrt{ML+1}\epsilon^{abs} + \epsilon^{rel}\|\rho_1\mathbf{u}\|_2$$

where ϵ^{abs} is a absolute tolerance and ϵ^{rel} is a relative tolerance.

We summarize the Algorithm 1 as follows.

Algorithm 1: Applying ADMM to Solve the Problem (17).

1) **Initialize**: $\mathbf{h}^0$, $\mathbf{r}^0$, $\mathbf{u}^0$, $\mathbf{v}^0$, ρ_1, ρ_2, and the tolerances ϵ^{abs} and ϵ^{rel}.
2) **While** the termination criterions in (37) is not satisfied **do**
3) Update $\mathbf{h}^{m+1}$ using (30).
4) Update $\mathbf{r}^{m+1}$ using (33).
5) Update $\mathbf{u}^{m+1}$ using (28).
6) Update $\mathbf{v}^{m+1}$ using (29).
7) m = m + 1.
8) **End while**

C. Analysis on Computational Complexity of the First Algorithm

It is important to evaluate the computational complexity of the Algorithm 1. For each update of $\mathbf{h}$, calculation of $\mathbf{\Xi}$ takes $\mathcal{O}(KM^2L^2)$, calculation of γ takes $\mathcal{O}(M^2L^2)$, so, the computational complexity of the update of $\mathbf{h}$ using (30) takes $\mathcal{O}(KM^2L^2+M^2L^2+M^3L^3)$. Similarly, the computational complexity of the update of $\mathbf{r}$ is $\mathcal{O}(KM^2L^2+M^2L^2+M^3L^3)$. Therefore, the computational complexity of Algorithm 1 is $\mathcal{O}(2(KM^2L^2+M^2L^2+M^3L^3))$ at each iteration.

IV. The Second Algorithm

In this section, the second algorithm is proposed to solve problem (18). We apply the double-ADMM (DADMM) approach to obtain a solution to (18).

In order to facilitate the analysis, we turn (18) to a real-value problem, by letting

$$\mathbf{r}_r \triangleq \begin{bmatrix}\mathrm{Re}\{\mathbf{r}\}\\ \mathrm{Im}\{\mathbf{r}\}\end{bmatrix},\ \mathbf{A}_r(\theta_k) \triangleq \begin{bmatrix}\mathrm{Re}\{\mathbf{A}(\theta_k)\} & -\mathrm{Im}\{\mathbf{A}(\theta_k)\}\\ \mathrm{Im}\{\mathbf{A}(\theta_k)\} & \mathrm{Re}\{\mathbf{A}(\theta_k)\}\end{bmatrix},$$
$$\bar{\mathbf{A}}_r(\theta_p,\theta_q) \triangleq \begin{bmatrix}\mathrm{Re}\{\bar{\mathbf{A}}(\theta_p,\theta_q)\} & -\mathrm{Im}\{\bar{\mathbf{A}}(\theta_p,\theta_q)\}\\ \mathrm{Im}\{\bar{\mathbf{A}}(\theta_p,\theta_q)\} & \mathrm{Re}\{\bar{\mathbf{A}}(\theta_p,\theta_q)\}\end{bmatrix}$$

and

$$\mathbf{E}_i^r \triangleq \begin{bmatrix}\mathrm{Re}\{\mathbf{E}_i\} & -\mathrm{Im}\{\mathbf{E}_i\}\\ \mathrm{Im}\{\mathbf{E}_i\} & \mathrm{Re}\{\mathbf{E}_i\}\end{bmatrix}$$

We can rewritten (18) as real-value problem,

$$\min_{\mathbf{r}} \frac{1}{K}\sum_{k=1}^{K}\omega_k\left|\mathbf{r}_r^T\mathbf{A}_r(\theta_k)\mathbf{r}_r\right| + \frac{\omega_c}{\bar{K}^2-\bar{K}}\sum_{p=1}^{\bar{K}-1}\sum_{q=p+1}^{\bar{K}}\left|\mathbf{r}_r^T\bar{\mathbf{A}}_r(\theta_p,\theta_q)\mathbf{r}_r\right|^2$$
$$s.t.\quad \mathbf{r}_r^T\mathbf{E}_{i+1}^r\mathbf{r} = 1, i = 1,2,\ldots,ML. \quad (39)$$

Analogous to the Algorithm 1, problem (39) is replaced by

$$\min_{\mathbf{r}_r,\mathbf{h}_r} \frac{1}{K}\sum_{k=1}^{K}\omega_k\left|\mathbf{h}_r^T\mathbf{A}_r(\theta_k)\mathbf{r}_r\right| + \frac{\omega_c}{\bar{K}^2-\bar{K}}\sum_{p=1}^{\bar{K}-1}\sum_{q=p+1}^{\bar{K}}\left|\mathbf{h}_r^T\bar{\mathbf{A}}_r(\theta_p,\theta_q)\mathbf{r}_r\right|^2$$
$$s.t.\quad \mathbf{h}_r-\mathbf{r}_r = \mathbf{0}$$
$$\mathbf{h}_r^T\mathbf{E}_{i+1}^r\mathbf{r}_r = 1, i = 1,2,\ldots,ML \quad (40)$$

Defining

$$\tilde{F}(\mathbf{h}_r,\mathbf{r}_r) = \frac{1}{K}\sum_{k=1}^{K}\omega_k\left|\mathbf{h}_r^T\mathbf{A}_r(\theta_k)\mathbf{r}_r\right| + \frac{\omega_c}{\bar{K}^2-\bar{K}}\sum_{p=1}^{\bar{K}-1}\sum_{q=p+1}^{\bar{K}}\left|\mathbf{h}_r^T\bar{\mathbf{A}}_r(\theta_p,\theta_q)\mathbf{r}_r\right|^2 \quad (41)$$

Let $\mathbf{\Theta}_k(\mathbf{h}_r) = \frac{\omega_k}{K}\mathbf{h}_r^T\mathbf{A}_r(\theta_k), k = 1,2,\cdots K$, and $\mathbf{\Theta}(\mathbf{h}_r) = [\mathbf{\Theta}_1(\mathbf{h}_r);\cdots;\mathbf{\Theta}_K(\mathbf{h}_r)] \in \mathbb{R}^{K\times 2(ML+1)}$, then (41) can be

Authorized licensed use limited to: UNIVERSITA MODENA. Downloaded on May 18,2024 at 12:47:07 UTC from IEEE Xplore. Restrictions apply.

written as follows:

$$\tilde{F}\left(\mathbf{h}_r,\mathbf{r}_r\right)=\|\boldsymbol{\Theta}(\mathbf{h}_r)\mathbf{r}_r\|_1 + \frac{\omega_c}{\bar{K}^2-\bar{K}}\sum_{p=1}^{\bar{K}-1}\sum_{q=p+1}^{\bar{K}}\left|\mathbf{h}_r^T\bar{\mathbf{A}}_r(\theta_p,\theta_q)\mathbf{r}_r\right|^2 \tag{42}$$

In addition, (41) can also be rewritten as

$$\tilde{F}\left(\mathbf{h}_r,\mathbf{r}_r\right)=\|\boldsymbol{\Phi}(\mathbf{r}_r)\mathbf{h}_r\|_1 + \frac{\omega_c}{\bar{K}^2-\bar{K}}\sum_{p=1}^{\bar{K}-1}\sum_{q=p+1}^{\bar{K}}\left|\mathbf{h}_r^T\bar{\mathbf{A}}_r(\theta_p,\theta_q)\mathbf{r}_r\right|^2 \tag{43}$$

where $\boldsymbol{\Phi}(\mathbf{r}_r)=[\boldsymbol{\Phi}_1(\mathbf{r}_r);\cdots;\boldsymbol{\Phi}_K(\mathbf{r}_r)]$, and $\boldsymbol{\Phi}_K(\mathbf{r}_r)=\frac{\omega_k}{K}\mathbf{r}_r^T\mathbf{A}_r^T(\theta_k), k=1,2,\cdots K$.

The augmented Lagrangian (using the scaled dual variables) is

$$\mathcal{L}(\mathbf{h}_r,\mathbf{r}_r,\mathbf{u},\mathbf{v})=\tilde{F}(\mathbf{h}_r,\mathbf{r}_r)+\frac{\rho_1}{2}\|\mathbf{h}_r-\mathbf{r}_r+\mathbf{u}\|_2^2 + \frac{\rho_2}{2}\|\mathbf{G}(\mathbf{h}_r,\mathbf{r}_r)+\mathbf{v}\|_2^2 \tag{44}$$

where $\mathbf{G}(\mathbf{h}_r,\mathbf{r}_r)$ is defined in (21). Inserting (21), (42) and (43) into (44) yields the scaled form of ADMM for this problem

$$\mathbf{h}_r^{m+1}:=\arg\min_{\mathbf{h}_r}\mathcal{L}(\mathbf{h}_r,\mathbf{r}_r^m,\mathbf{u}^m,\mathbf{v}^m) \tag{45}$$

$$\mathbf{r}_r^{m+1}:=\arg\min_{\mathbf{r}_r}\mathcal{L}(\mathbf{h}_r^{m+1},\mathbf{r}_r,\mathbf{u}^m,\mathbf{v}^m) \tag{46}$$

$$\mathbf{u}^{m+1}:=\mathbf{u}^m+\mathbf{h}_r^{m+1}-\mathbf{r}_r^{m+1} \tag{47}$$

$$\mathbf{v}^{m+1}:=\mathbf{v}^m+\mathbf{G}(\mathbf{h}_r^{m+1},\mathbf{r}_r^{m+1}) \tag{48}$$

In the following, we present solutions to the update of $\mathbf{h}_r$ and $\mathbf{r}_r$ using the ADMM algorithm.

A. *Update of* $\mathbf{h}_r$

The update of $\mathbf{h}_r$ involves solving the unconstrained problem (45), which can be split into two functions: a nonsmooth function and a smooth function. Hence, we can find its solution through the ADMM approach. we rewrtie (45) as follows:

$$\begin{aligned}\min_{\mathbf{x},\mathbf{h}_r}\ &\|\mathbf{x}\|_1+\frac{\omega_c}{\bar{K}^2-\bar{K}}\sum_{p=1}^{\bar{K}-1}\sum_{q=p+1}^{\bar{K}}\left|\mathbf{h}_r^T\bar{\mathbf{A}}_r(\theta_p,\theta_q)\mathbf{r}_r^m\right|^2 \\ &+\frac{\rho_1}{2}\|\mathbf{h}_r-\mathbf{r}_r^m+\mathbf{u}^m\|_2^2+\frac{\rho_2}{2}\|\mathbf{T}'(\mathbf{r}_r^m)\mathbf{h}_r-\mathbf{1}+\mathbf{v}^m\|_2^2 \\ s.t.\ \ &\boldsymbol{\Phi}(\mathbf{r}_r^m)\mathbf{h}_r-\mathbf{x}=\mathbf{0}\end{aligned} \tag{49}$$

Therefore, we can formulate the ADMM form of (49)

$$\mathbf{h}_r^{n+1}:=\arg\min_{\mathbf{h}_r}\left\{\begin{array}{l}\frac{\omega_c}{\bar{K}^2-\bar{K}}\sum_{p=1}^{\bar{K}-1}\sum_{q=p+1}^{\bar{K}}|\mathbf{h}_r^T\bar{\mathbf{A}}_r \\ \quad\times(\theta_p,\theta_q)\mathbf{r}_r^m|^2 \\ +\frac{\rho_1}{2}\|\mathbf{h}_r-\mathbf{r}_r^m+\mathbf{u}^m\|_2^2 \\ +\frac{\rho_2}{2}\|\mathbf{T}'(\mathbf{r}_r^m)\mathbf{h}_r-\mathbf{1}+\mathbf{v}^m\|_2^2 \\ +\frac{\rho_3}{2}\|\boldsymbol{\Phi}(\mathbf{r}_r^m)\mathbf{h}_r-\mathbf{x}^n+\mathbf{w}^n\|_2^2\end{array}\right\} \tag{50}$$

$$\mathbf{x}^{n+1}:=\arg\min_{\mathbf{x}}\left\{\|\mathbf{x}\|_1+\frac{\rho_3}{2}\|\boldsymbol{\Phi}(\mathbf{r}_r^m)\mathbf{h}_r^{n+1}-\mathbf{x}+\mathbf{w}^n\|_2^2\right\} \tag{51}$$

$$\mathbf{w}^{n+1}:=\mathbf{w}^n+\boldsymbol{\Phi}(\mathbf{r}_r^m)\mathbf{h}_r^{n+1}-\mathbf{x}^{n+1} \tag{52}$$

where $\rho_3>0$ is a penalty parameter, and $\mathbf{w}$ is the scaled dual variable.

It is easy to obtain a closed-form solution to (50), that is

$$\mathbf{h}_r^{n+1}:=\boldsymbol{\Gamma}^{-1}\boldsymbol{\eta} \tag{53}$$

where

$$\begin{aligned}\boldsymbol{\Gamma}=&\left(\frac{2\omega_c}{\bar{K}^2-\bar{K}}\sum_{p=1}^{\bar{K}-1}\sum_{q=p+1}^{\bar{K}}\bar{\mathbf{A}}_r(\theta_p,\theta_q)\mathbf{r}_r^m\mathbf{r}_r^{m\,T}\bar{\mathbf{A}}_r^T(\theta_p,\theta_q)\right) \\ &+\rho_1\mathbf{I}+\rho_2\mathbf{T}'^T(\mathbf{r}_r^m)\mathbf{T}'(\mathbf{r}_r^m)+\rho_3\boldsymbol{\Phi}^T(\mathbf{r}_r^m)\boldsymbol{\Phi}(\mathbf{r}_r^m)\end{aligned}$$

and

$$\begin{aligned}\boldsymbol{\eta}=&\rho_1(\mathbf{r}_r^m-\mathbf{u}^m)+\rho_2\mathbf{T}'^T(\mathbf{r}_r^m)(\mathbf{1}-\mathbf{v}^m) \\ &+\rho_3\boldsymbol{\Phi}^T(\mathbf{r}_r^m)(\mathbf{x}^n-\mathbf{w}^n)\end{aligned}$$

Lemma 2: A closed-form solution to (51) also can be obtained by

$$\mathbf{x}^{n+1}:=S_{1/\rho_3}\left(\boldsymbol{\Phi}(\mathbf{r}_r^m)\mathbf{h}_r^{n+1}+\mathbf{w}^n\right) \tag{54}$$

where the soft thresholding operator S is defined as

$$S_k(a)=\begin{cases}a-k & a>k\\ 0 & |a|\le k\\ a+k & a-k\end{cases}$$

Proof: The proof is provided in Appendix B. ■

B. *Update of* $\mathbf{r}_r$

Due to the symmetry of $\mathbf{r}_r$ and $\mathbf{h}_r$, we can obtain the solution of the update $\mathbf{r}_r$ in (46) similar to the update $\mathbf{h}_r$ in (45).

C. *Termination Criterions of the Second Algorithm*

The primal residuals and the dual residual, respectively, are

$$\begin{aligned}d_{r1}^{m+1}&=\mathbf{h}_r^{m+1}-\mathbf{r}_r^{m+1},\\ d_{r2}^{m+1}&=\mathbf{T}'(\mathbf{r}_r^{m+1})\mathbf{h}_r^{m+1}-\mathbf{1}\end{aligned} \tag{55}$$

and

$$d_s^{m+1}=\rho_1(\mathbf{r}_r^{m+1}-\mathbf{r}_r^m) \tag{56}$$

Authorized licensed use limited to: UNIVERSITA MODENA. Downloaded on May 18,2024 at 12:47:07 UTC from IEEE Xplore. Restrictions apply.

The termination criterions of the second algorithm are similar to (38), and the tolerances for primal residuals and dual residual are

$$\epsilon_1^{pri} = \sqrt{2ML\ +\ 2}\epsilon^{abs} + \epsilon^{rel}\max\{\|\mathbf{h}_r^m\|_2, \|-\mathbf{r}_r^m\|_2\}$$
$$\epsilon_2^{pri} = \sqrt{ML}\epsilon^{abs} + \epsilon^{rel}\max\{\|\mathbf{T}(\mathbf{h}_r^m)\mathbf{r}_r^m\|_2, \|-\mathbf{1}\|_2\}$$
$$\epsilon^{dual} = \sqrt{2ML\ +\ 2}\epsilon^{abs} + \epsilon^{rel}\|\rho_1\mathbf{u}\|_2$$

The DADMM algorithm for solving the problem (18) is summarized in Algorithm 2.

Algorithm 2: Applying DADMM to Solve the Problem (18).

1) **Initialize**: $\mathbf{h}_r^0$, $\mathbf{r}_r^0$, $\mathbf{u}^0$, $\mathbf{v}^0$, $\mathbf{w}^0$, ρ_1, ρ_2, ρ_3 and the tolerances ϵ^{abs} and ϵ^{rel}.
2) **While** the termination criterions is not satisfied **do**
3) Update $\mathbf{h}_r^{m+1}$ in (45) using the ADMM algorithm.
4) Update $\mathbf{r}_r^{m+1}$ in (46) using the ADMM algorithm.
5) Update $\mathbf{u}^{m+1}$ using (47).
6) Update $\mathbf{v}^{m+1}$ using (48).
7) m = m + 1.
8) **End while**

D. Analysis on Computational Complexity of the Second Algorithm

We also examine the computational complexity of the second algorithm (*i.e.* the DADMM algorithm). For each update of primal variable $\mathbf{h}_r$, we need to solve (45) via the ADMM approach. In the ADMM framework, the update of $\mathbf{h}_r$ (*i.e.* solving (50)) takes $\mathcal{O}(M^3L^3)$, the update of $\mathbf{x}$ (*i.e.* solving (51)) takes $\mathcal{O}(ML)$, and the update of $\mathbf{w}$ takes $\mathcal{O}(M^2L^2)$. Then, solving (45) will take $\mathcal{O}(\log(\frac{1}{\epsilon})(M^3L^3 + ML + M^2L^2))$ [30], where ϵ is a given accuracy of the ADMM approach. Similarly, solving (46) will also take $\mathcal{O}(\log(\frac{1}{\epsilon})(M^3L^3 + ML + M^2L^2))$. Therefore, the computational complexity of Algorithm 2 is $\mathcal{O}(2\log(\frac{1}{\epsilon})(M^3L^3 + ML + M^2L^2))$ at each iteration.

V. Numerical Results

In this section, we present some numerical examples to evaluate the performance of the ADMM-based constant modulus waveform design algorithms for MIMO radar. In all of the following numerical simulations, we consider a uniform linear array (ULA) of $M = 10$ elements with half-wavelength inter-element interval, and each transmit pulse has $L = 32$ samples. The range of angle is $(-90^\circ, 90^\circ)$ with spacing 1°, and the weight for the k-th angle $\omega_k = 1, k = 1, 2, \ldots, K$ (unless otherwise stated), and $\omega_c = 0$, same as [19]. We first provide some examples to illustrate the effectiveness of the first algorithm. Then we compare the performance of the beampattern synthesized by using the first algorithm to that of the second algorithm via several examples.

Besides, all the numerical examples are analysed using Matlab 2012b version, perfoming on a standard PC (with CPU Core i3 3.1 GHz and 4 GB of RAM).

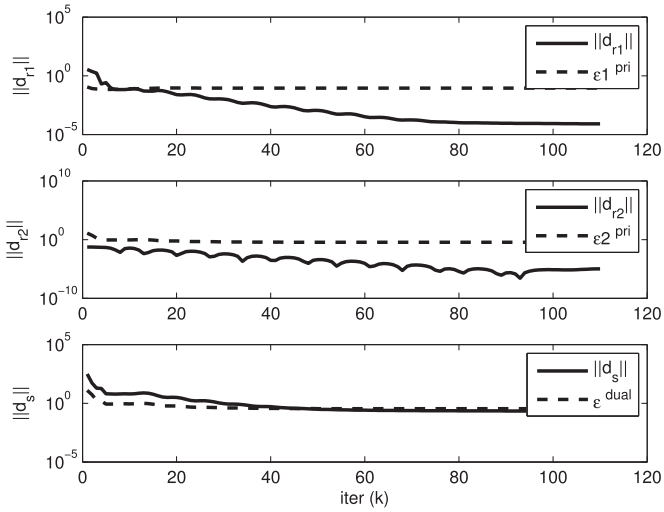

Fig. 2. Norms of primal residuals and dual residual versus the iteration number when $\rho_1 = \rho_2 = 20$.

A. The First Algorithm

In the first example, we consider a desired beampattern with three main lobes at $\theta_1 = -40^\circ$, $\theta_2 = 0^\circ$, $\theta_3 = 40^\circ$, and each width of them is $\Delta\theta = 20^\circ$. The desired beampattern is

$$d(\theta) = \begin{cases} 1, & \theta \in \left[\theta_k - \dfrac{\Delta\theta}{2},\ \theta_k + \dfrac{\Delta\theta}{2}\right],\ k = 1, 2, 3 \\ 0, & \text{otherwise} \end{cases}$$

We choose the squared-error cost function to design the waveform. The larger penalty parameter will enforce the constant modulus condition more strongly, so the primal residuals in (36) are smaller, but the dual residual in (37) is larger, Since convergence of the proposed algorithm requires both small primal residuals and dual residual (*i.e.* inequalities in (38) hold). In this paper, we set all the penalty parameters to the same, $\rho_1 = \rho_2 = 20$. The absolute tolerance and relative tolerance are $\epsilon^{abs} = 10^{-3}$ and $\epsilon^{rel} = 10^{-2}$, respectively. The variables $\mathbf{h}^0$, $\mathbf{u}^0$ and $\mathbf{v}^0$ are initialized to be zero vector, and the variable $\mathbf{r}^0$ is initialized to be random vector (Notice that the algorithm can converge to global optimal solution for any $\mathbf{r}^0$, except for zero vector).

The primal and dual residual norms, as well as the corresponding stopping criterion limits ϵ_1^{pri}, ϵ_2^{pri} and ϵ^{dual} versus the iteration number are shown in Fig. 2. The stopping conditions are met after 50 iterations, but we ran the proposed algorithm for 110 iterations to display the following process.

Fig. 3 reveals the objective function values in (9) versus the iteration number (ignoring the constant term $1/K$). As illustrated in Fig. 3, the objective function is minimised after 8 iterations. However, the constant modulus condition is satisfied after 50 iterations, which is illustrated in Fig. 4, indicating that the synthesized waveform by the first proposed algorithm meets the constraint requirement as the iterative process goes on.

Fig. 5 shows the result of the beampattern matching design through the proposed first approach. For comparison, the optimal covariance matrix $\mathbf{R}$ in [19], the waveform matrix $\mathbf{X}$ via cyclic algorithm (CA) in [20], and the DFT-based method in

Authorized licensed use limited to: UNIVERSITA MODENA. Downloaded on May 18,2024 at 12:47:07 UTC from IEEE Xplore. Restrictions apply.

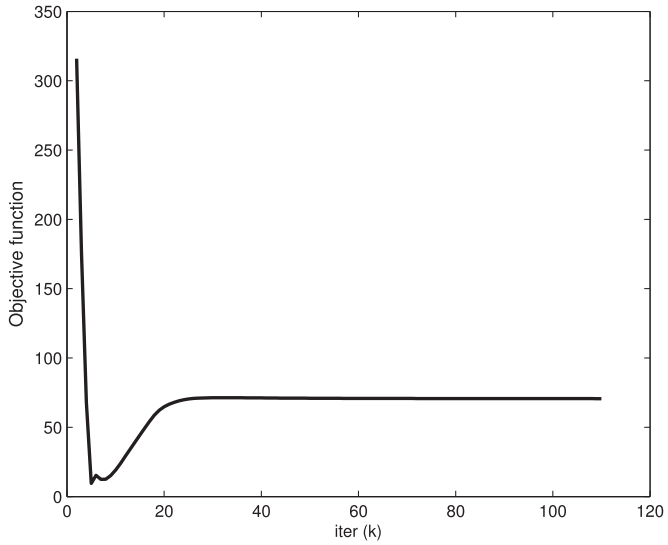

Fig. 3. The objective function values in (9) versus iteration when $\rho_1 = \rho_2 = 20$.

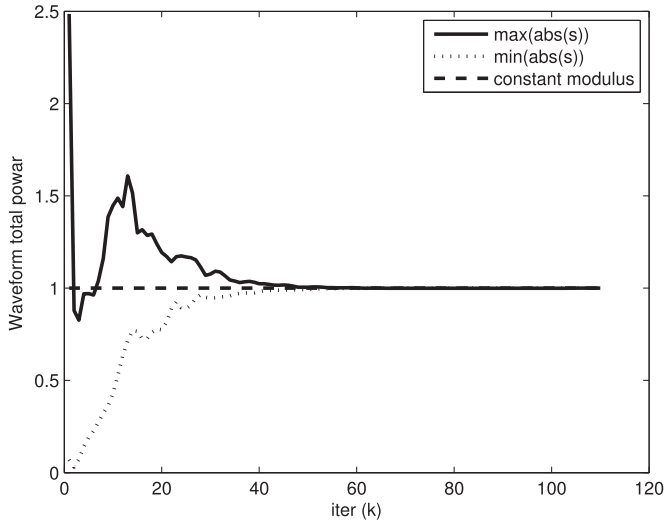

Fig. 4. The waveform modulus versus iteration. The solid line shows the maximum amplitude of the designed waveform, the dotted line shows the minimum amplitude.

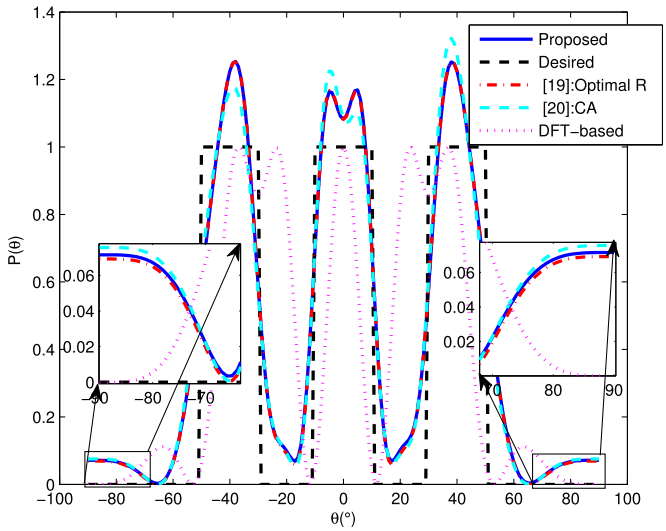

Fig. 5. The three main lobes beampattern with width $\Delta\theta = 20°$.

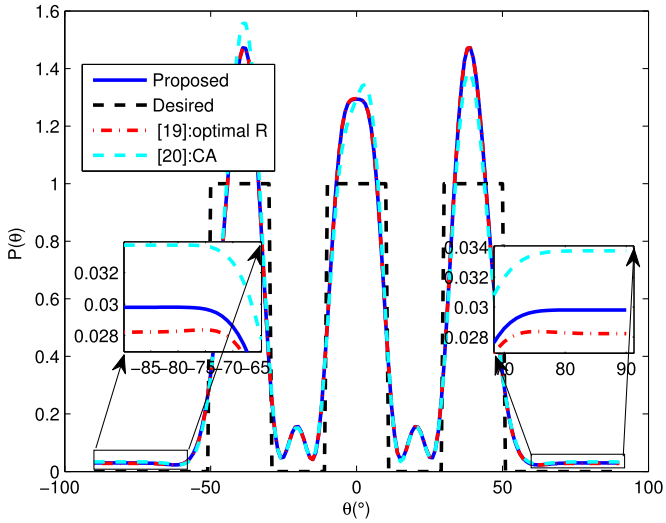

Fig. 6. Transmit beampatterns synthesized via the proposed first algorihtm, $\mathbf{R}$ in [19] and $\mathbf{X}$ in [20] when $w_k = 5$ in the side-lobe-levels and $w_k = 1$ in the region-of-interest.

[22]–[24] are also considered in Fig. 5. The results illustrate that the beampattern obtained by the first proposed approach is very close to that using the optimal $\mathbf{R}$, and more effective than the waveform matrix $\mathbf{X}$ in [20]. Unfortunately, due to the small number of antennas, the DFT-based method can not achieve good beampattern matching performance. Remarkably, the first proposed algorithm can find the transimit signal waveform directly, rather than two-step approach discussed in [19] and [20].

Next, we also evaluate the low sidelobe characteristics of the designed beampattern by the proposed first method when $w_k = 5$ in the side-lobe-levels and $w_k = 1$ in the region-of-interest. Compared with results in Figs. 5 and 6 shows that the synthesized beampattern in this case has a better sidelobe performance than that with $\omega_k = 1, k = 1, 2, \ldots, K$. As expected, Fig. 6 also illustrates that the beampattern synthesized by the proposed first method is very similar to that of the method in [19].

In addition, we discuss the influence of different penalty parameters on convergence of the first algorithm. Convergence performance results with different fixed penalty parameters are compared in the Fig. 7. The result shows that, when the penalty parameters are $\rho_1 = 20, \rho_2 = 20$, the objective function converges faster than the other values.

In the second example, we consider a desired beampattern with one main lobe at $\theta = 0°$, and its width is $\Delta\theta = 60°$. Other parameters are same as in the first example. As expected, results in Fig. 8 also show that the first proposed algorithm can well approximate the beampattern obtained through the optimal $\mathbf{R}$ in [19].

Finally, Table I summarizes the performance of the proposed first algorithm, optimal $\mathbf{R}$ in [19], $\mathbf{X}$ in [20] and the DFT-based method in [22]–[24], in terms of the mean-squared error (MSE)

Authorized licensed use limited to: UNIVERSITA MODENA. Downloaded on May 18,2024 at 12:47:07 UTC from IEEE Xplore. Restrictions apply.

TABLE I
THE MSES, ROUGH COMPLEXITY OF EACH ITERATION AND GLOBAL COMPUTATION TIME (SECONDS) OF THE PROPOSED FIRST ALGORITHM, OPTIMAL $\mathbf{R}$, WAVEFORM MATRIX $\mathbf{X}$ AND THE DFT-BASED METHOD WITH $\omega_k = 1, k = 1, 2, \ldots, K$

	Complexity	Computation time	MSE	
			The first case	The second case
The first algorithm	$\mathcal{O}(M^3L^3)$	7.12	0.0382	0.0089
$\mathbf{R}$ in [19]	$\mathcal{O}(M^{3.5})$[22]	4.32	0.0379	0.0086
$\mathbf{X}$ in [20]	$\mathcal{O}(M^{3.5}) + \mathcal{O}(M^3)$[20]	6.62	0.0391	0.0102
DFT-based method	$\mathcal{O}(M\log(M))$[24]	0.36	0.1964	0.099

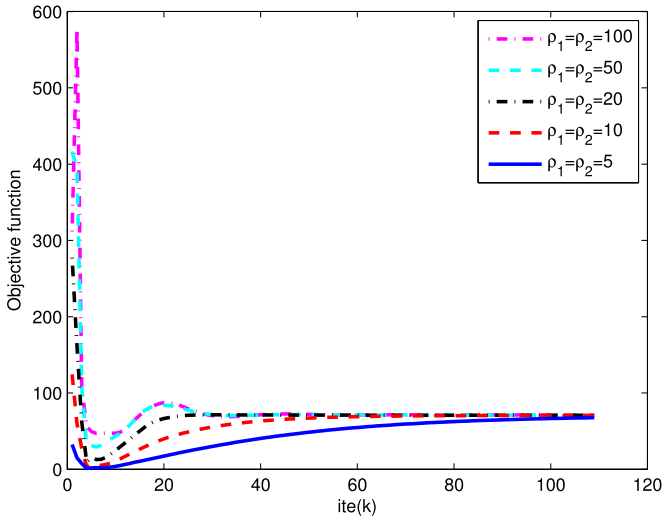

Fig. 7. The influence of different penalty parameters on convergence of the objective function.

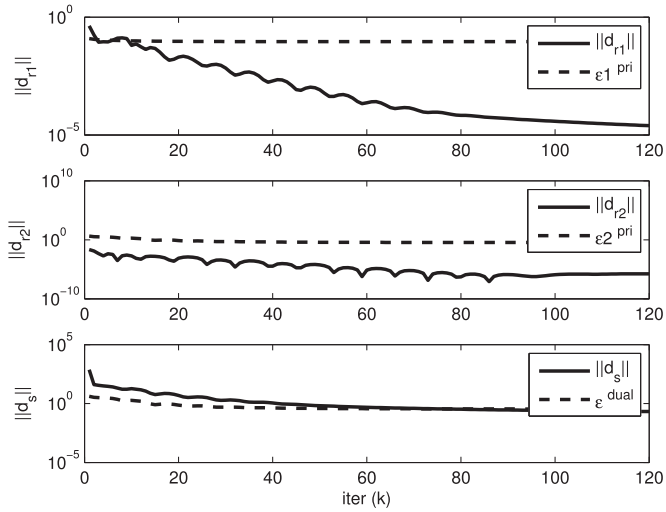

Fig. 9. Norms of primal residuals and dual residual versus the iteration number when $\rho_1 = \rho_2 = 20$, and $\rho_3 = 1$.

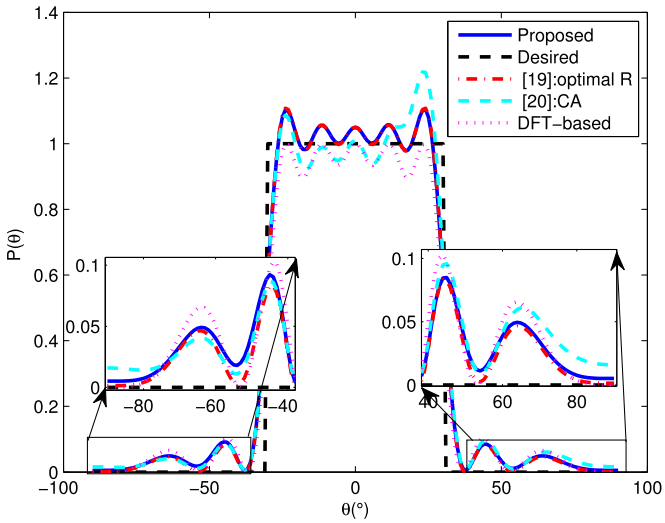

Fig. 8. The one main lobe beampattern with width $\Delta\theta = 60°$.

between the desired beampattern and the synthesized beampattern under two cases (*i.e.* a desired beampattern with three main lobes and one main lobe are considered, respectively.), rough complexity of each iteration and global computation time.

Define the MSE as

$$\text{MSE} = \frac{1}{K}\sum_{k=1}^{K}[P(\theta_k) - d(\theta_k)]^2,$$

where $P(\theta_k)$ is the normalized desired beampattern. Results in Table I also show that, comparing to other methods, the MSE performance of the proposed first algorithm is closer to that of the optimal $\mathbf{R}$ in [19].

B. The Second Algorithm

In this subsection, we compare the beampattern design by the first algorithm with that of the second algorithm. We set the penalty parameters $\rho_1 = \rho_2 = 20$, and $\rho_3 = 1$. The absolute tolerance and relative tolerance are same as in the first algorithm.

Similarly, we first verify the convergence performance of the second algorithm when a desired beampattern with three main lobes at $\theta_1 = -40°, \theta_2 = 0°, \theta_3 = 40°$ is considered. Results in Fig. 9 show that the stopping conditions of the second algorithm are met after about 80 iterations. Meanwhile, Fig. 10 exhibits that the objective function of the second algorithm can converge to the global optimum.

Next, Fig. 11 compares the beampattern synthesized based on the second algorithm with that of the first algorithm. Results show that the former approach has a comparable or better sidelobe performance than the later, meaning that the second

Authorized licensed use limited to: UNIVERSITA MODENA. Downloaded on May 18,2024 at 12:47:07 UTC from IEEE Xplore. Restrictions apply.

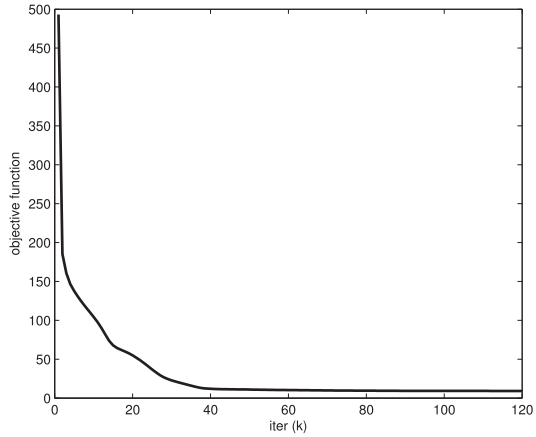

Fig. 10. The objective function values in (14) versus iteration when $\rho_1 = \rho_2 = 20$, and $\rho_3 = 1$.

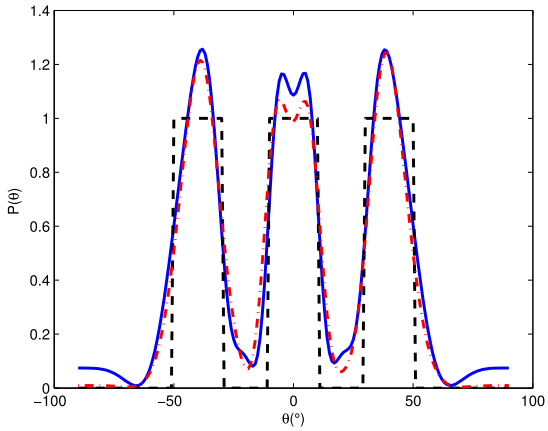

Fig. 11. The three mainlobes beampattern designed by using the first algorithm and the second algorithm. The black dash-dash line shows the desired pattern, the blue solid line show the first algorithm, the red dash-dot shows the second algorithm.

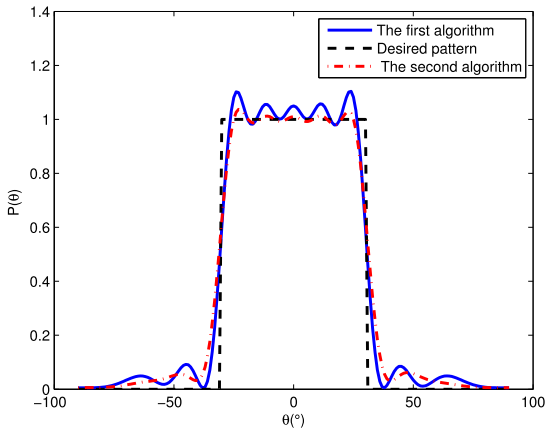

Fig. 12. The one mainlobe beampattern designed by using the first algorithm and the second algorithm.

algorithm is more suitable than the first algorithm for matching the desired beampattern.

Finally, Fig. 12 compares the performance of the first algorithm to that of the second algorithm for the case where a one mainlobe (whose width is $\Delta\theta = 60^\circ$) symmetric beampattern is desired. Fig. 12 displays that the beampattern designed via the second algorithm has a better performance than that obtained by the first algorithm.

VI. Conclusion

In this paper, the problem of transmit beampattern matching design is addressed for a colocated MIMO radar system. Two one-step algorithms are proposed to design the transmit waveform under the constant modulus constraint. In the first algorithm, the squared-error between the designed beampattern and the given beampattern is chosen as the cost function. We have solved the original nonconvex fourth-order problem by using the ADMM approach. Meanwhile, the first proposed algorithm provides a new method for solving the class of optimization problems involving a nonconvex fourth-order polynomial objective function and nonconvex quadratic equality constraints.

The absolute-error is adopted as the cost function in the second algorithm, and then we have applied the DADMM algorithm to solve it. Finally, numerical examples indicate that the first proposed algorithm can achieve almost the same performance as the optimal $\mathbf{R}$ in [19]. Further, the second algorithm can perform better beampattern design than the first algorithm.

Possible future work might include the waveform design subject to low autocorrelation sidelobes and spectral constraints [39]. In addition, joint design of spectrum sharing between a MIMO radar and a MIMO communication system [40] might be interesting.

Appendix A
Proof of the Lemma 1

To find the global minimization of (26), we need to take the derivative of (26) with respect to $\mathbf{h}^*$, and let the derivative be zero vector $i.e.$,

$$\mathbf{0} = \nabla_{\mathbf{h}^*}\mathcal{L}(\mathbf{h}, \mathbf{r}^m, \mathbf{u}^m, \mathrm{v}^m) \tag{57}$$

From the equation (22), we have

$$\nabla_{\mathbf{h}^*}F(\mathbf{h}, \mathbf{r}^m) = \left(\frac{1}{K}\sum_{k=1}^{K}\omega_k\mathbf{A}(\theta_k)\mathbf{r}^m\mathbf{r}^{m\,\dagger}\mathbf{A}^\dagger(\theta_k)\right)\mathbf{h} + \left(\frac{\omega_c}{\bar{K}^2-\bar{K}}\sum_{p=1}^{\bar{K}-1}\sum_{q=p+1}^{\bar{K}}\bar{\mathbf{A}}(\theta_p,\theta_q)\mathbf{r}^m\mathbf{r}^{m\,\dagger}\bar{\mathbf{A}}^\dagger(\theta_p,\theta_q)\right)\mathbf{h} \tag{58}$$

$$\nabla_{\mathbf{h}^*}\|\mathbf{h} - \mathbf{r}^m + \mathbf{u}^m\|_2^2 = \mathbf{h} - (\mathbf{r}^m - \mathbf{u}^m) \tag{59}$$

and

$$\nabla_{\mathbf{h}^*}\|\mathbf{T}'(\mathbf{r}^m)\mathbf{h} - \mathbf{1} + \mathbf{v}^m\|_2^2 = \mathbf{T}'^{\dagger}(\mathbf{r}^m)\mathbf{T}'(\mathbf{r}^m)\mathbf{h} - \mathbf{T}'^{\dagger}(\mathbf{r}^m)(\mathbf{1} - \mathbf{v}^m) \tag{60}$$

Authorized licensed use limited to: UNIVERSITA MODENA. Downloaded on May 18,2024 at 12:47:07 UTC from IEEE Xplore. Restrictions apply.

Hence,

$$\begin{aligned}\nabla_{\mathbf{h}^*}\mathcal{L}(\mathbf{h},\mathbf{r}^m,\mathbf{u}^m,\mathrm{v}^m) &= \nabla_{\mathbf{h}^*}F(\mathbf{h},\mathbf{r}^m)\\ &+ \frac{\rho_1}{2}\nabla_{\mathbf{h}^*}\|\mathbf{h}-\mathbf{r}^m+\mathbf{u}^m\|_2^2\\ &+ \frac{\rho_2}{2}\nabla_{\mathbf{h}^*}\|\mathbf{T}'(\mathbf{r}^m)\mathbf{h}-\mathbf{1}+\mathbf{v}^m\|_2^2\\ &= \Xi\mathbf{h}-\gamma=\mathbf{0} \end{aligned} \tag{61}$$

where Ξ and γ are defined in (31) and (32), respectively. Then we have,

$$\mathbf{h}=\Xi^{-1}\gamma \tag{62}$$

Therefore, the (30) is proved. Similarly, the (33) can be also proved.

Appendix B
Proof of the Lemma 2

To find the global minimization of (51), we consider the i-th element of the vector $\mathbf{s}$. Letting

$$\mathbf{q}=\mathbf{\Phi}(\mathbf{r}_r^m)\mathbf{h}_r+\mathbf{w}^n$$

In the case of x_i-update is

$$x_i^+ := \arg\min_{x_i}\left(|x_i|+\frac{\rho_3}{2}(x_i-q_i)^2\right) \tag{63}$$

1). When $x_i>0$, the extreme value of the following function

$$x_i+\frac{\rho_3}{2}(x_i-q_i)^2$$

is $q_i-\frac{1}{\rho_3}$. So, i) $q_i>\frac{1}{\rho_3}$, x_i can take the extreme point, $i.e.$ $x_i=q_i-\frac{1}{\rho_3}$; ii) $q_i\le\frac{1}{\rho_3}$, the minimum point is $x_i=0$.

2). When $x_i\le 0$, we need to find the extreme value of the following function

$$-x_i+\frac{\rho_3}{2}(x_i-q_i)^2$$

In this case, the update of x_i is similar to the case 1).

To summarize, the solution to (63) is

$$x_i^+ := S_{1/\rho_3}(q_i) \tag{64}$$

Therefore, the (54) is proved.

References

[1] E. Fishler, A. Haimovich, R. Blum, D. Chizhik, L. Cimini, and R. Valenzuela, "MIMO radar: An idea whose time has come," in *Proc. IEEE Radar Conf.*, Apr. 2004, pp. 71–78.

[2] D. R. Fuhrmann and G. S. Antonio, "Transmit beamforming for MIMO radar systems using partial signal correlation," in *Proc. 38th Asilomar Conf. Signals, Syst. Comput.*, Nov. 2004, vol. 1, pp. 295–299.

[3] E. Fishler, A. Haimovich, R. Blum, L. Cimini, D. Chizhik, and R. Valenzuela, "Performance of MIMO radar systems: Advantages of angular diversity," in *Proc. 38th Asilomar Conf. Signals, Syst. Comput.*, Nov. 2004, vol. 1, pp. 305–309.

[4] F. Robey, S. Coutts, D. Weikle, J. McHarg, and K. Cuomo, "MIMO radar theory and experimental results," in *Proc. 38th Asilomar Conf. Signals, Syst., Comput.*, Pacific Grove, CA, USA, Nov. 2004, pp. 300–304.

[5] K. Forsythe and D. Bliss, "Waveform correlation and optimization issues for MIMO radar," in *Proc. 39th Asilomar Conf. Signals, Syst. Comput.*, Nov. 2005, pp. 1306–1310.

[6] A. Haimovich, R. Blum, and L. Cimini, "MIMO radar with widely separated antennas," *IEEE Signal Process. Mag.*, vol. 25, no. 1, pp. 116–129, Jan. 2008.

[7] E. Fishler, A. Haimovich, and R. Blum, "Spatial diversity in radars-models and detection performance," *IEEE Trans. Signal Process.*, vol. 54, no. 3, pp. 823–838, Aug. 2007.

[8] Q. He, R. S. Blum, H. Godrich, and A. M. Haimovich, "Target velocity estimation and antenna placement for MIMO radar with widely separated antennas,"*J. Sel. Top. Signal Process.*, vol. 4, no. 1, pp. 79–100, Feb. 2010.

[9] J. Li and P. Stoica, "MIMO radar with colocated antennas," *IEEE Signal Process. Mag.*, vol. 24, no. 5, pp. 106–114, Sep. 2007.

[10] J. Li, and P. Stoica, *MIMO Radar Signal Processing*. New York, NY, USA: Wiley, 2008.

[11] Y. Chen, Y. Nijsure, C. Yuen, Y. H. Chew, Z. Ding, and S. Boussakta, "Adaptive distributed MIMO radar waveform optimization based on mutual information," *IEEE Trans. Aerosp. Electron. Syst.*, vol. 49, no. 2, pp. 1374–1385, 2013.

[12] Y. Yang and R. S. Blum, "MIMO radar waveform design based on mutual information and minimum meansquare error estimation," *IEEE Trans. Aerosp. Electron. Syst.*, vol. 43, no. 1, pp. 330–343, Jan. 2007.

[13] G. Cui, H. Li, and M. Rangaswamy, "MIMO radar waveform design with constant modulus and similarity constraints," *IEEE Trans. Signal Process.*, vol. 62, no. 2, pp. 343–353, Jun. 2014.

[14] O. Aldayel, V. Monga, and M. Rangaswamy, "Successive QCQP refinement for MIMO radar waveform design under practical constraints," *IEEE Trans. Signal Process.*, vol. 64, no. 14, pp. 3760–3774, Jul. 2016.

[15] B. Jiu, H. Liu, and X. Wang, "Knowledge-based spatial-temporal hierarchical MIMO radar waveform design method for target detection in heterogeneous clutter zone," *IEEE Trans. Signal Process.*, vol. 63, no. 3, pp. 543–554, Feb. 2015.

[16] S. Ahmed and M. Alouini, "MIMO radar waveform covariance matrix for high SINR and low side-lobe levels," *IEEE Trans. Signal Process.*, vol. 62, no. 8, pp. 2056–2065, Apr. 2014.

[17] S. Sen, "PAPR-constrained pareto-optimal waveform design for OFDM-STAP radar," *IEEE Trans. Geosci. Remote Sens.*, vol. 52, no. 6, pp. 3658–3669, Jun. 2014.

[18] G. Cui, X. Yu, V. Carotenuto, and L. Kong, "Space-time transmit code and receive filter design for colocated MIMO radar," *IEEE Trans. Signal Process.*, vol. 65, no. 5, pp. 1116–1129, 2017.

[19] P. Stoica, J. Li, and Y. Xie, "On probing signal design for MIMO radar," *IEEE Trans. Signal Process.*, vol. 55, no. 8, pp. 4151–4160, Aug. 2007.

[20] P. Stoica, J. Li, and X. Zhu, "Waveform synthesis for diversity-based transmit beampattern design," *IEEE Trans. Signal Process.*, vol. 56, no. 6, pp. 2593–2598, Jun. 2008.

[21] J. Li, P. Stoica, and X. Zheng, "Signal synthesis and receiver design for MIMO radar imaging," *IEEE Trans. Signal Process.*, vol. 56, no. 8, pp. 3959–3968, Aug. 2008.

[22] J. Lipor, S. Ahmed, and M. M. Alouini, "Fourier-based transmit beampattern design using MIMO radar," *IEEE Trans. Signal Process.*, vol. 62, no. 9, pp. 2226–2235, Apr. 2014.

[23] T. Bouchoucha, S. Ahmed, T. Y. Naffouri, and M. S. Alouini, "Closed-form solution to directly design FACE waveforms for beampatterns using planar array," in *Proc. IEEE Int. Conf. Acoust., Speech, Signal Process.*, 2015, pp. 2359–2363.

[24] T. Bouchoucha, S. Ahmed, and M. S. Alouini, "DFT-based closed-form covariance matrix and direct waveforms design for MIMO radar to achieve desired beampatterns," *IEEE Trans. Signal Process.*, vol. 62, no. 9, pp. 2104–2113, Jan. 2017.

[25] S. Ahmed, J. Thompson, and Y. Petillot, "Unconstrained synthesis of covariance matrix for MIMO radar transmit beampattern," *IEEE Trans. Signal Process.*, vol. 59, no. 8, pp. 3837–3849, Aug. 2011.

[26] X. Zhang, Z. He, L. Bacchus, and J. Yan, "MIMO radar transmit beampattern matching design," *IEEE Trans. Signal Process.*, vol. 63, no. 8, pp. 2049–2056, Apr. 2015.

[27] Z. Cheng, Z. He, R. Li, and Z. Wang, "Robust transmit beampattern matching synthesis for MIMO radar," *Electron. Lett.*, vol. 53, no. 9, pp. 620–622, 2017.

[28] H. He, J. Li, and P. Stoica, *Waveform Design for Active Sensing Systems—A Computational Approach*. Cambridge, U.K.: Cambridge Univ. Press, 2012.

[29] S. Ahmed, J. S. Thompson, Y. R. Petillot, and B. Mulgrew, "Finite alphabet constant-envelope waveform design for MIMO radar," *IEEE Trans. Signal Process.*, vol. 59, no. 11, pp. 5326–5337, Nov. 2011.

Authorized licensed use limited to: UNIVERSITA MODENA. Downloaded on May 18,2024 at 12:47:07 UTC from IEEE Xplore. Restrictions apply.

[30] S. Boyd and L. Vandenberghe, *Convex Optimization.* Cambridge, U.K.: Cambridge Univ. Press, 2004.
[31] S. Boyd, N. Parikh, E. Chu, B. Peleato, and J. Eckstein, "Distributed optimization and statistical learning via the alternating direction method of multipliers," *Found, Trends Mach. Learn.*, vol. 3, no. 1, pp. 1–122, 2011.
[32] D. P. Bertsekas and J. N. Tsitsiklis, *Parallel and Distributed Computation: Numerical Methods*. Upper Saddle River, NJ, USA: Prentice-Hall, 1989.
[33] Z. Chen, R. Molin, and A. K. Katsaggelos, "Robust recovery of temporally smooth signals from under-determined multiple measurements," *IEEE Trans. Signal Process.*, vol. 63, no. 7, pp. 1779–1791, Apr. 2015.
[34] M. Hong, Z. Luo, and M. Razaviyayn, "Convergence analysis of alternating direction method of multipliers for a family of nonconvex problems," in *Proc. IEEE Int. Conf. Acoust., Speech, Signal Process.*, 2015, pp. 3836–3840.
[35] Z. Cheng *et al.*, "Alternating direction method of multipliers for MIMO radar waveform design," in *Proc. IEEE Radar Conf.*, May, 2017, pp. 0367–0371.
[36] M. Grant and S. Boyd, CVX: Matlab software for disciplined convex programming, version 2.1, Feb. 2016. [Online] Available: http://cvxr.com/cvx
[37] Z. Luo, W. Ma, A. So, Y. Ye, and S. Zhang, "Semidefinite relaxation of quadratic optimization problems," *IEEE Signal Process. Mag.*, vol. 27, no. 3, pp. 20–34, May 2010.
[38] A. B. Gershman, N. D. Sidiropoulos, S. Shahhazpanahi, M. Bengtsson, and B. Ottersten, "Convex optimization-based beamforming: From receive to transmit and network designs," *IEEE Signal Process. Mag.*, vol. 27, no. 3, pp. 62–75, May 2010.
[39] W. Rowe, P. Stoica, and J. Li, "Spectrally constrained waveform design, *IEEE Signal Process. Mag.*, vol. 31, no. 3, pp. 157–162, May 2014.
[40] B. Li, A. Petropulu, and W. Trappe, "Optimum co-design for spectrum sharing between matrix completion based MIMO radars and a MIMO communication system," *IEEE Trans. Signal Process.*, vol. 64, no. 17, pp. 4562–4575, 2016.

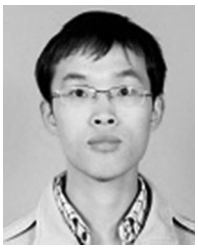

Ziyang Cheng was born in Yingcheng, Hubei, China, in 1990. He has received the M.S. degree in circuits and systems from the University of Electronic Science and Technology of China (UESTC), Chengdu, China, in 2015. He is currently working toward the Ph.D. degree in signal and information processing at the UESTC. His research interests include array signal processing, MIMO radar waveform design, radar target detection, and optimization theory.

Zishu He (M'11) was born in Chengdu, Sichuan province, China, in 1962. He received the B.S., M.S., and Ph.D. degree in signal and information processing from the University of Electronic Science and Technology of China (UESTC), Chengdu, China, in 1984, 1988, and 2000, respectively.

Currently he is a Professor in the school of electronic engineering of UESTC. His current research interests include array signal processing, digital beam forming, the theory on MIMO radar, and adaptive signal processing. He has finished more than two hundred papers and has written two books.

Shengmiao Zhang has received the B.S. and Ph.D degrees from the School of Electronic Engineering, University of Electronic Science and Technology of China, Chengdu, China, in 2010 and 2016, respectively. She is currently an Engineer with Science and Technology on Electronic Information Control Laboration. Her research interests include space-time adaptive processing and knowledge aided radar signal processing.

Jian Li (M'91–SM'97–F'05) received the M.Sc. and Ph.D. degrees in electrical engineering from Ohio State University, Columbus, OH, USA, in 1987 and 1991, respectively.

She is currently a Professor in the Department of Electrical and Computer Engineering, University of Florida, Gainesville, FL, USA. Her current research interests include spectral estimation, statistical and array signal processing, and their applications to radar, sonar, and biomedical engineering. Her publications include Robust Adaptive Beamforming (2005, Wiley), Spectral Analysis: The Missing Data Case (2005, Morgan & Claypool), MIMO Radar Signal Processing (2009, Wiley), and Waveform Design for Active Sensing Systems—A Computational Approach (2011, Cambridge University Press). She is a Fellow of IET. She received the 1994 National Science Foundation Young Investigator Award and the 1996 Office of Naval Research Young Investigator Award. She was an Executive Committee Member of the 2002 International Conference on Acoustics, Speech, and Signal Processing, Orlando, FL, USA, May 2002. She was an Associate Editor of the IEEE TRANSACTIONS ON SIGNAL PROCESSINGfrom 1999 to 2005, an Associate Editor of the IEEE SIGNAL PROCESSING MAGAZINE from 2003 to 2005, and a member of the Editorial Board of Signal Processing, a publication of the European Association for Signal Processing, from 2005 to 2007. She was a member of the Editorial Board of the IEEE Signal Processing Magazine from 2010 to 2012. She is currently a member of the Sensor Array and Multichannel Technical Committee of the IEEE Signal Processing Society. She is a coauthor of the paper that has received the M. Barry Carlton Award for the best paper published in IEEE Transactions on Aerospace and Electronic Systems in 2005. She is also a coauthor of a paper published in IEEE Transactions on Signal processing that has received the Best Paper Award in 2013 from the IEEE Signal Processing Society.

Authorized licensed use limited to: UNIVERSITA MODENA. Downloaded on May 18,2024 at 12:47:07 UTC from IEEE Xplore. Restrictions apply.